Chemosphere 177 (2017) 266–274

Contents lists available at ScienceDirect

Chemosphere

journal homepage: www.elsevier.com/locate/chemosphere

Sea salt sodium record from Talos Dome (East Antarctica) as a potential proxy of the Antarctic past sea ice extent

M. Severi [a, *], S. Becagli [a], L. Caiazzo [a], V. Ciardini [b], E. Colizza [c], F. Giardi [a], K. Mezgec [c], C. Scarchilli [b], B. Stenni [d], E.R. Thomas [e], R. Traversi [a], R. Udisti [a, f]

[a] University of Florence, Chemistry Dept. "Ugo Schiff", Via della Lastruccia, 3, 50019, Sesto Fiorentino, FI, Italy
[b] Laboratory for Earth Observations and Analyses, ENEA, Rome, Italy
[c] Department of Mathematics and Geosciences, University of Trieste, Trieste, Italy
[d] Department of Environmental Sciences, Informatics and Statistics, "Ca' Foscari" University of Venice, Italy
[e] British Antarctic Survey, Cambridge, UK
[f] ISAC CNR, Via Gobetti 101, 40129, Bologna, Italy

HIGHLIGHTS

- Sea salt sodium at Talos Dome can be used as a reliable proxy of sea ice extent.
- A positive relationship between $ssNa^{+}$ flux and SIE maxima was found.
- SIE of the Ross Sea and Western Pacific was reconstructed over the 20th century.
- SIE variability increased starting from 1990s.

GRAPHICAL ABSTRACT

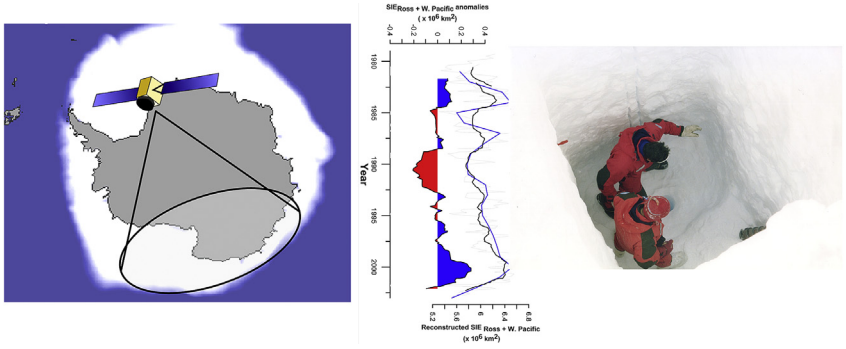

ARTICLE INFO

Article history:
Received 7 October 2016
Received in revised form
17 February 2017
Accepted 7 March 2017
Available online 8 March 2017

Handling Editor: J. de Boer

Keywords:
Sea-ice
Ice-core
Antarctica
Paleo reconstruction
Climate change
Ross Sea

ABSTRACT

Antarctic sea ice has shown an increasing trend in recent decades, but with strong regional differences from one sector to another of the Southern Ocean. The Ross Sea and the Indian sectors have seen an increase in sea ice during the satellite era (1979 onwards). Here we present a record of $ssNa^{+}$ flux in the Talos Dome region during a 25-year period spanning from 1979 to 2003, showing that this marker could be used as a potential proxy for reconstructing the sea ice extent in the Ross Sea and Western Pacific Ocean at least for recent decades. After finding a positive relationship between the maxima in sea ice extent for a 25-year period, we used this relationship in the TALDICE record in order to reconstruct the sea ice conditions over the 20th century. Our tentative reconstruction highlighted a decline in the sea ice extent (SIE) starting in the 1950s and pointed out a higher variability of SIE starting from the 1960s and that the largest sea ice extents of the last century occurred during the 1990s.

* Corresponding author.
E-mail address: mirko.severi@unifi.it (M. Severi).

http://dx.doi.org/10.1016/j.chemosphere.2017.03.025
0045-6535/

1. Introduction

Sea-ice represents a powerful phenomenon exerting a strong influence on the oceanic, biological and climatic systems and, given its importance, it is a focus in environmental research. The expansion and retreat of Antarctic sea-ice is one of the most striking seasonal changes affecting the Earth today, effectively increasing by two fold the surface area of Antarctica (Allen et al., 2011). Sea-ice plays a key role in the production and upkeep of deep waters in the ocean and therefore in the whole global ocean circulation system (Dieckmann and Hellmer, 2010). Moreover, sea-ice greatly affects the transfer of energy at the ocean-atmosphere interface as it shows a much higher albedo with respect to open water (Brandt et al., 2005) and is thus able to reflect more incoming radiation deeply changing the radiative balance. The presence of sea-ice also represents a physical barrier that successfully inhibits the transfer of heat, moisture and trace gases (such as CO_2) between the ocean and the atmosphere (Bopp et al., 2003). Additionally sea-ice has a direct influence on the Antarctic biota and it has been suggested that it is linked to the "biological pump" and thus to the global carbon cycle (Sarmiento and Gruber, 2006).

For all these reasons, despite an unknown exact mechanism, sea-ice plays a critical role in the polar amplification of climate change (Serreze and Barry, 2011) and, therefore, it is important to predict changes in sea ice under the future conditions of an ongoing climate change. A better understanding of the links between sea-ice and climate and a real improvement of the models requires a large series of long observational datasets. Unfortunately, satellite observations only began in the 1970s and before that we rely on sporadic observations and proxy data. (Abram et al., 2013).

The reconstructions of Antarctic sea-ice cover used as data for the parameterization of models have been so far mainly based on diatom remains found in marine sediment cores (Armand et al., 2005, 2008). These diatom based reconstructions can provide quantitative estimates of yearly sea-ice presence and/or duration and can allow us to draw limits for winter and summer sea-ice extents (Esper and Gersonde, 2014). Particularly large datasets have been made available based on the occurrence of sea-ice related diatoms (Gersonde et al., 2005) and, in the last years, new methods based on a sea-ice biomarker known as IP_{25} have been developed (Belt et al., 2007; Belt and Müller, 2013) in order to reconstruct the Arctic sea-ice cover in the past. In more recent years, the analysis of an organic geochemical lipid biomarker, called $IPSO_{25}$, has been proposed as a possible proxy measure of Antarctic sea ice (Massé et al., 2011; Collins et al., 2013).

Ice cores drilled in the Antarctic ice-sheet represent a very different kind of proxy record with respect to ocean sediment cores. The information about sea-ice is present in the ice cores only if it is transported from the surface of the ocean to the atmosphere. The information about sea ice is transported from the surface of the ocean to the atmosphere and unlike the sediment records is representative of sea ice in a particular sector, rather a single site. One of the greatest advantages of using ice cores to reconstruct sea-ice variations is their higher temporal resolution with respect to marine sediment cores. Reconstruction of sea-ice from ice-core proxies have so far been based on concentrations or fluxes of sodium, methanesulphonic acid (MSA, $CH_3SO_3^-$) and, more recently, halogen species.

Sea salt sodium ($ssNa^+$) has been used to quantify sea-ice variations (Wolff et al., 2006) based on the formation of high salinity "frost flowers" and brine (Rankin et al., 2000) on sea ice surfaces. However, a recent laboratory experiment (Roscoe et al., 2011) shows that frost flowers are very stable also in the presence of wind and no significant aerosol emission was observed. For this reason, such source of $ssNa^+$ is difficult to distinguish from other dominating sources, such as sea spray aerosol, which has been proved to be dominant at many drilling sites, e.g. James Ross Island (Abram et al., 2011) and Law Dome (Curran et al., 1998). Yang et al. (2008) proposed more recently that a massive source of Na^+ in several Antarctic drilling sites could be represented by "blowing snow", i.e. the snow lying on sea ice, rich in salts, that can be easily lifted into the air through blowing-snow events. Levine et al. (2014) found in their model experiment that, on an interannual scale, meteorology, and not sea ice extent, is the dominant control on the atmospheric concentration of sea salt. Which is the real factor controlling the sea salt content in Antarctic sites is so far still an open and debated question.

Methanesulphonic acid (MSA) was first used quantitatively for a reconstruction of sea ice extent (SIE hereafter) by Curran et al. (2003) in an ice-core drilled at Law Dome. Afterwards this marker has been largely investigated as a sea-ice proxy in several drilling sites (Abram et al., 2010; Becagli et al., 2009, 2016; Foster et al., 2006; Criscitiello et al., 2013) highlighting both positive and negative relationship between MSA and sea ice. However, this compound is not always fully stable in snow and ice and can be easily remobilised in the ice matrix after deposition (Smith et al., 2004) limiting its utility for long-term sea ice reconstructions at certain sites.

Recently, two halogens, namely iodine and bromine, has been suggested as ice core proxies useful to reconstruct the past sea ice concentration at Talos Dome (Spolaor et al., 2013) and at Law Dome (Vallelonga et al., 2016); furthermore the Canadian Arctic sea ice was successfully reconstructed for the last 120.000 years from the NEEM ice core (Greenland) using the bromine content as a proxy (Spolaor et al., 2016).

In this paper we assess the suitability of $ss\text{-}Na^+$ at Talos Dome (TD here hence) as a proxy for past sea ice conditions. The reliability of the sea salt sodium record from Talos Dome site in serving as a potential proxy of SIE is supported by the comparison between the $ssNa^+$ stratigraphic profile and the calculation of sea ice extent achieved by satellite data in the 1979–2003 time period.

Severi et al. (2009) showed already the relationship between Na^+ and SOI (Southern Oscillation Index) and the good agreement between $nssSO_4^{2-}$ and MSA with the anomalies in SIE for the 1975–1995 period suggesting the potential of this site in recording variations in sea ice and sea ice-related parameters. The results obtained from the analysis of a 5.65 m snowpit give further support for the use of $ssNa^+$ as qualitative sea-ice tracer at the TALDICE drilling site, where sea-spray deposition and fractionation effects have been deeply investigated in the past (Becagli et al., 2004; Traversi et al., 2004).

2. Materials and methods

2.1. Sampling site

Talos Dome is a coastal dome (Fig. 1) in Northern Victoria Land on the edge of the East Antarctic plateau and is located about 290 km from the Southern Ocean (Oates Land–George V Land), 250 km from the Ross Sea, and 275 km from the Italian "Mario Zucchelli" Station (Terra Nova Bay). The site chosen for digging a snow-pit (159° 10′ 30.9″ E, 72° 49′ 04.6″ S, 2330 m a.s.l.) was close to the centre of the dome and also to the TALDICE deep drilling site (Stenni et al., 2011; Severi et al., 2012).

During the 2003/2004 Antarctic campaign a snow pit was dug by hand to a depth of 565 cm and more than 200 samples were continuously collected along a vertical line using pre-cleaned PET vials with a mean resolution of 2.5 cm, wearing sterile overalls and gloves. All the samples were then stored in sealed polyethylene bags and kept frozen in insulated boxes for the transport to Italy.

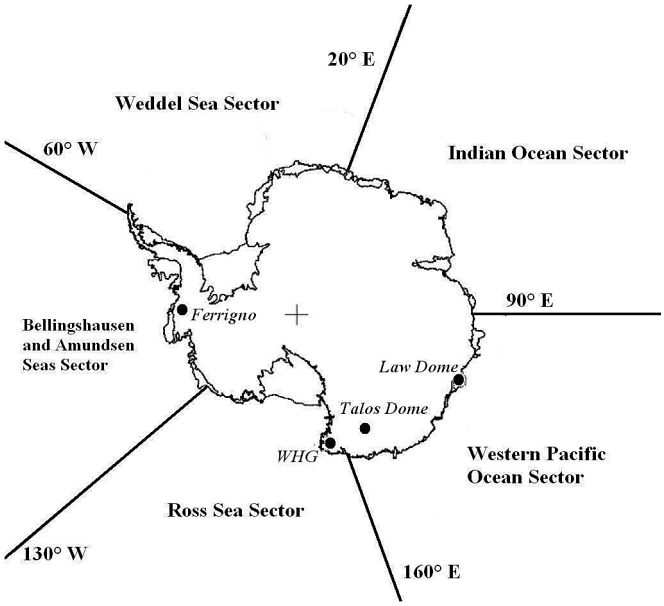

Fig. 1. Map of the Antarctic continent showing Talos Dome, Law Dome, Ferrigno and Whitehall Glacier sites and the division in five sectors of the Southern Ocean as in Cavalieri and Parkinson (2008).

2.2. Analysis method

The samples were melted in a clean room under a class-100 laminar flow hood shortly before chemical analysis. The method used for the analysis of the ionic content of the samples was based on a fully automated ion chromatographic system described in details elsewhere (Caiazzo et al., 2016; Morganti et al., 2007; Severi et al., 2009).

Na^+ content in Antarctic aerosol, and thus snow and ice, is always dominated by sea salt, especially in interglacial periods, showing a minor contribution of dust leachable Na^+. As an example, the non-sea salt contribution to Na^+ total budget at Dome C during the Holocene was estimated to be around 2% (Röthlisberger et al., 2002) and therefore Na^+ direct measurement could be reasonably taken as a marker of sea salt. Nonetheless, the "pure" sea salt contribution can be more reliably assessed if the mineral dust contribution to Na^+ content is cut off. Therefore, we corrected the total Na^+ content using non sea-salt Ca^{2+} ($nssCa^{2+}$) as crustal marker and a simple two-variable, two-equation system allowing the evaluation of the ss- and nss-fractions of both Na^+ and Ca^{2+}:

$$1)\ ssNa^+ = totNa^+ - nssCa^{2+}/R_{crust}$$

$$2)\ nssCa^{2+} = Ca^{2+} - R_{sea\ water} * ssNa^+$$

$$(Ca^{2+}/Na^+ = 0.038 = R_{sea\ water})\ (Ca^{2+}/Na^+ = 1.78 = R_{crust})$$

where R_{crust} and $R_{sea\ water}$ are the mean ratio (w/w) in the Earth crust and in bulk seawater, respectively (Bowen, 1979). For the TD site, on average only 5% of the total Na^+ does not come from sea spray.

The snow pit was dated by annual layer counting, using a multi-parametric approach as described in Severi et al. (2009). Using this kind of dating in our record, we cannot exclude misinterpretation in the annual layers counting or missing years in the snow layers due to wind ablation of the snow layers and low accumulation (Frezzotti et al., 2007). In order to minimize these type of errors we smoothed our annual data with a 3-year running average, indeed we have to take into account a possible dating error of 2/3 years.

In order to account for the dilution of the original atmospheric aerosol concentrations in the snow pit samples by snow accumulation, the measured concentrations had to be corrected for this effect. This was achieved by multiplying the measured concentrations by the accumulation rate at the respective depth or age, resulting in the total deposition flux of the aerosol (Wolff et al., 2006). The accumulation rate along the snow pit was calculated according to the age scale of Severi et al. (2009) and to the density profile of the snow pit achieved using the method described in Severi et al. (2009). Following this methodology the annual $ssNa^+$ flux was calculated by multiplying the mean annual concentration values by the annual accumulation rates at the TD site.

A high resolution $ssNa^+$ flux time series for TD site, spanning the last century (2003–1920 DC), was built by overlapping the TALDICE ice core Na^+ record and the snowpit data. The TALDICE deep ice core started at a depth of 5.0 m and we used our high resolution (2.5 cm) snow pit data to fill the missing top part of the core. The TALDICE Na^+ flux (at 4 cm resolution) was calculated using the past accumulation rates modelled in the AICC2012 age scale (Bazin et al., 2013; Veres et al., 2013) at 1 m resolution.

2.3. Sea ice extent (SIE) data

Time series of the monthly mean sea ice extent for each region of the Southern Ocean (Weddell Sea, Indian Ocean, Western-Pacific Ocean, Ross Sea and Bellingshausen and Amundsen Seas) spanning from November 1979 to December 2003, were calculated from observations of sea ice concentrations from passive microwave satellite radiometers (Sea Ice Concentrations from Nimbus-7 SMMR and DMSP SSM/I-SSMIS Passive Microwave Data) (Parkinson and Cavalieri, 2012).

Sea ice concentration is published at a regular 25 km resolution daily. The ice extent is calculated by summing the areas of the pixels within each region with ice concentrations of at least 15% and then averaged on a monthly basis.

2.4. Back-trajectories (TJ) air masses

Three-day back trajectories were computed daily, arriving at 1000 m and 3000 m over TD at 12UTC. The backward trajectories were generated using the Hybrid Single-Particle Lagrangian Integrated Trajectory (HYSPLIT) model developed by NOAA and Australia's Bureau of Meteorology (Draxler and Rolph, 2012), for the period spanning from 1979 to 2003, covering completely the snowpit time range. HYSPLIT is initialised with the European Centre for Medium Range Weather Forecast (ECMWF) ERA Interim Reanalysis meteorological data fields (Simmons et al., 2006) with a regular grid of $1^\circ \times 1^\circ$. Errors in TJ calculations after 3 days are estimated in the range 10–20% of the travel distance (Schlosser et al. (2008), Scarchilli et al. (2011)). The TJs were projected onto the Sea Ice Cover (SIC) field, and the nearest model value was associated with hourly SIC value along the trajectory path, assuming a constant ice cover condition during the day.

2.5. Climatic indexes

Our analysis takes into account the Inter-decadal Pacific Oscillation (IPO) and the Antarctic Oscillation (AAO), in order to better understand the possible linkage between SIE and $ssNa^+$ flux at TD.

IPO is a naturally fluctuating atmospheric pressure which is responsible of warming or cooling of sea surface temperature (SST) over the entire Pacific Basin. Each IPO cycle can last from 20 to 30 years (Salinger et al., 2001). Since the latest 1990s the IPO index has

been in a "negative phase", causing a decrease of SST and, as a consequence, sea ice to rapidly increase. In our analysis we used the dataset available online at https://data.mfe.govt.nz/x/ReypdH.

The circulation variability of the lower atmosphere in the Southern Hemisphere is triggered by the annular mode in the pressure field anomaly at various temporal time, from seasonal to inter-annual (Thompson and Wallace, 2000). This mode has been referred to as the Antarctic Oscillation (AAO), or the Southern Annular Mode (SAM) and it is significantly related to the strength of the westerlies and storm track around Antarctica (Baldwin, 2001); we used the dataset described in Marshall (2003) in order to discuss the relationship between SIE and $ssNa^+$ flux data.

3. Results

Fig. 2 shows the maximum values of SIE for two selected sectors of the Southern Ocean (Ross Sea and Western Pacific Ocean) and for the total Antarctic continent in the time period spanning from 1979 to 2003. On average, over this 25-year period, maximum SIE occurs in September for all sectors; hence, we refer in our work to the SIE maxima as the September monthly average in each year. For the total Antarctic sea ice, the SIE maxima range from a minimum of 17.7×10^6 km^2 in 1986 to a maximum of 18.9×10^6 km^2 in 1998. We applied a linear regression to the September monthly average values for the Antarctic total SIE and for the two selected sectors of the Southern Ocean (see bold lines in Fig. 2). The trend of the September Antarctic SIE shows a positive slope in agreement with previous results (Parkinson and Cavalieri, 2012) confirming that in the studied period there is a general trend to the increase of the SIE for the Southern hemisphere The SIE maxima of the Western Pacific Ocean (90°E – 160°E) shows a slightly decreasing trend whereas the Ross Sea sector (160°E – 130°W) shows a positive trend of the September SIE trend. In summary we can assess that, while there is a general increase of SIE at continental scale in Antarctica mostly driven by the Ross Sea sector, the variations of the SIE around the continent are different from one sector to another of the Southern Ocean, showing both positive and negative trends (Parkinson and Cavalieri, 2012; Jones et al., 2016).

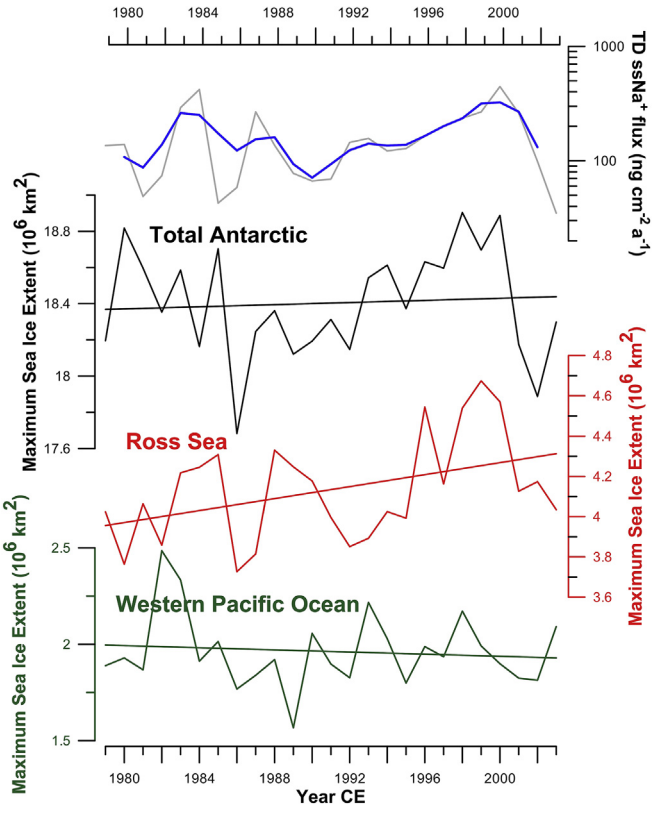

Fig. 2. Maximum September Sea Ice Extent (calculated as monthly average) from 1979 to 2003 as reconstructed from satellite measurement for the Western Pacific Ocean (green) and the Ross Sea (red) sectors of the Southern Ocean. The total Antarctic SIE is shown as a black line and it is calculated as the sum of the five sectors shown in Fig. 1. For each sector the trend of the September SIE over the 25-year period is also shown as a solid line. The top panel shows the profile of the $ssNa^+$ flux at Talos Dome as yearly mean values (light grey line) and as three-year running mean (blue line). (For interpretation of the references to colour in this figure legend, the reader is referred to the web version of this article.)

The top panel of Fig. 2 shows the $ssNa^+$ flux measured in the Talos Dome snow pit. A simple 3-years running average is superposed in order to minimize dating errors due to low accumulation and post depositional phenomena. A general agreement with the maximum SIE of the whole continent is evident; for example there is an increase both in the $ssNa^+$ flux and in the SIE starting from the beginning of the 1990s. The comparison with the SIE of each sector of the Southern Ocean shows less evident common features even if some similarities between $ssNa^+$ flux and maximum SIE appear for the Ross Sea sector.

The spatial correlation between smoothed $ssNa^+$ flux and Sea Ice Cover (SIC) and ECMWF era Interim Geopotential Height at 500 hPa (GP), during March–November (MAMJJASON) are highlighted in Fig. 3. Both SIC and GP fields are smoothed with a 3-year running average in order to be consistent with smoothed $ssNa^+$ flux time series. The comparison with SIC shows relative high correlation (Fig. 3a) in the Ross Sea, in the Western Pacific Sector and along

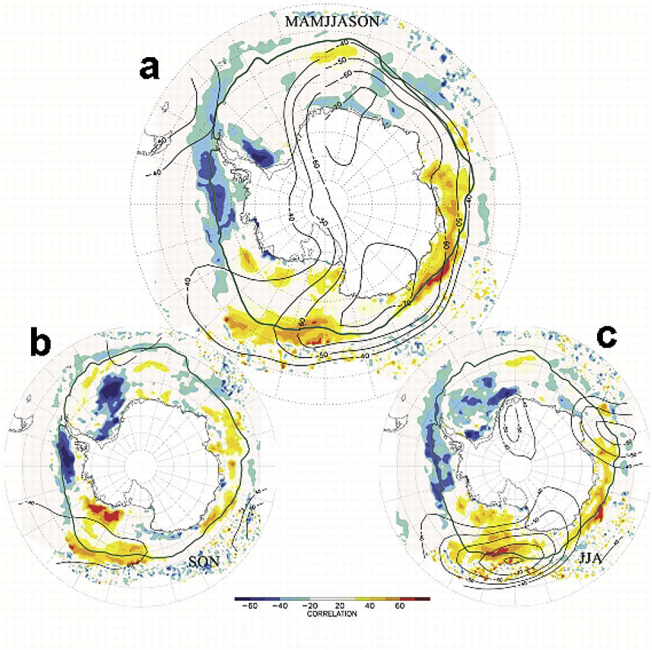

Fig. 3. Spatial correlation between 3 year running averaged ssNa+ from TD snow pit and 3 year running averaged Sea Ice Concentration (SIC, filled contour) and 500 hPa geopotential height (GP500, black lines contour). Panel a shows correlation between $ssNa^+$ annual values and SIC and GP500 averaged over the period March, April, May, June, July, August, September, October and November (MAMJJASON) time series. Panel b shows correlation between $ssNa^+$ annual values and SIC and GP500 averaged over the period September, October and November (SON) time series. Panel c shows correlation between $ssNa^+$ annual values and SIC and GP500 averaged over the period June, July, August (JJA) time series. Green line represents Sea Ice Concentration at 0.20 contour as proxy of seasonal Sea Ice extension limit. (For interpretation of the references to colour in this figure legend, the reader is referred to the web version of this article.)

Wilkes Land at the boundaries of the sea ice edge where sea ice variability is greatest. On the other hand strong anti-correlation appears in the Bellingshausen sea, along the Antarctic Peninsula coasts and in the Weddell sea.

The correlation with the GP shows a large negative feature spread over East Antarctica and extending to southern oceans and Ross Sea with a large minimum above Oates and Wilkes lands. These correlations are enhanced during winter period (JJA, Fig. 3c) where most of SIC over Ross Sea and Western Pacific seems positively correlated to Na^+ flux with maxima along the sea ice edge. Particularly interesting is the JJA spatial correlation with GP which is no more elongated over all the East Plateau but it is now concentrated over the Ross Sea sector with a centre of action above the maximum correlation between Na^+ flux and SIC. These features are probably connected to the increasing (decreasing) of storm track passage over Southern Ocean between 150° E and 150°W and consequently decreasing (increasing) in pressure and geopotential fields and enhance (suppress) of $ssNa^+$ advection to Talos Dome site.

In order to understand possible $ssNa^+$ path from source regions toward the TD site, we selected TJ which show along their path at least three points where interpolated SIC and wind speed are greater than 0.50 and 5 m/s, respectively, and the altitudes are comprised between 50 and 500 m above the ground. The TJ analysis in Fig. 4 suggests that the provenance of air masses, possibly related to $ssNa^+$ transport to TD, are mainly from the Western Pacific and Ross Sea sectors (130°W-130E°). TJ ending at 1000 m above TD generally encounter favorable conditions for loading Na^+ close to the Antarctic coasts of Oates, Victoria and Marie Byrd Lands and Ross Sea. On the other hand TJs ending at 3000 m above TD generally meet loading conditions off-shore, with loads prevalently over Southern Ocean between 70° and 65°S close to the sea ice edge. The selected TJs are mainly distributed over winter months and partly during the end of autumn and beginning of spring. Sala et al. (2008), using a similar analysis but with slightly different conditions, highlighted the same loading areas with preferences of the Ross Sea sector during fall and spring and from the Southern and Indian Ocean sectors during winter.

Spatial correlation and TJs analysis point out that formation and variability of the sea ice over the entire Ross Sea and Western Pacific Ocean sectors, especially during winter months, could be connected to $ssNa^+$ flux as measured at TD site. For this reason we selected the whole Ross Sea and Western Pacific sectors as the most probable source areas of $ssNa^+$ and we investigated the role of $ssNa^+$ at Talos Dome as a sea ice proxy.

Fig. 5a shows the September SIE maxima from 1979 to 2003 as the sum of the Ross Sea and the Western Pacific Ocean sectors September SIE maxima (dark red line) and the $ssNa^+$ annual mean

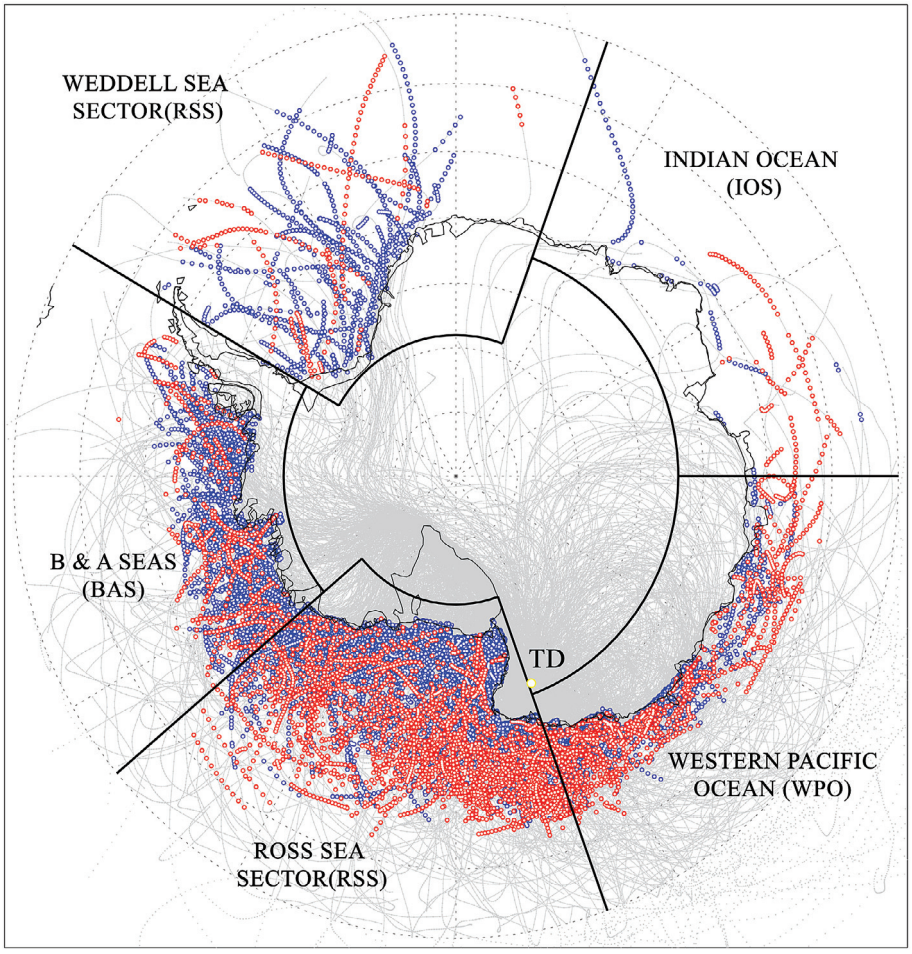

Fig. 4. Three-day back-trajectories (TJ) for the period 1979–2003 arriving at 1000 m and 3000 m over TD at 12UTC (grey lines) generated using HYSPLIT model and related to possible $ssNa^+$ loads. Blue and red points show where the selected TJs arriving at 1000 and 3000 m above TD, respectively, meet loading criteria (at least 3 points along the path where Sea Ice cover (SIC) > 0.50, 10 m Wind Speed (WS) > 5 m/s and 50 < TJ height < 500 m above the ground). Black lines highlight ocean sectors boundaries, Ross Sea (RSS), Western Pacific Ocean (WPO), Indian Ocean (IOS), B&A Seas (BAS) and Weddell Sea (WSS), as defined by Parkinson and Cavalieri (2012). (For interpretation of the references to colour in this figure legend, the reader is referred to the web version of this article.)

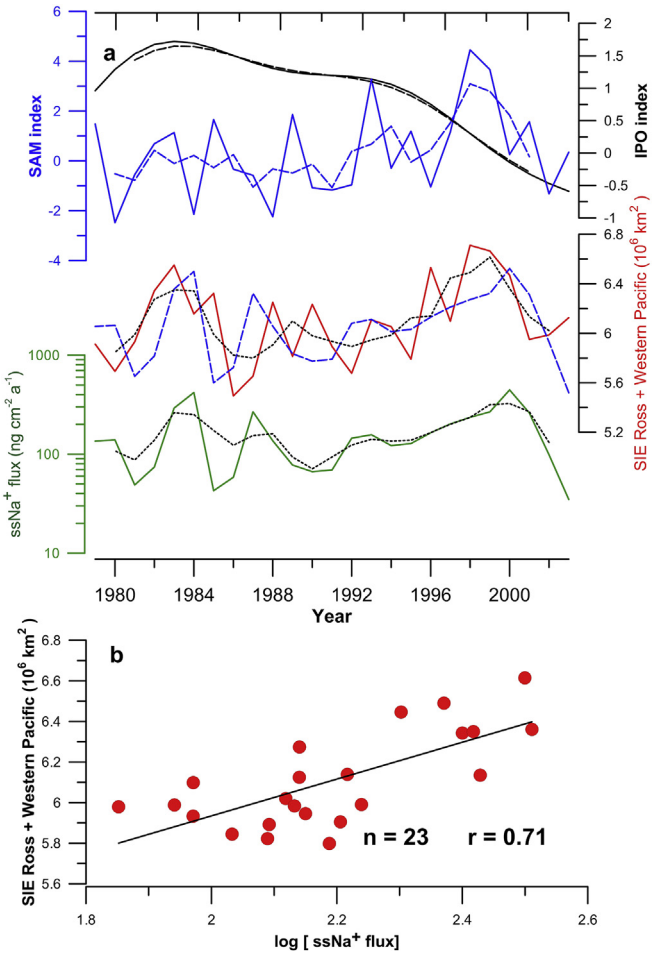

Fig. 5. **(a)** Yearly average ssNa + flux (in ng cm^{-2} a^{-1}) between 1979 and 2003 as measured in the Talos Dome snow pit (green line). For the same period the Sea Ice Extent as the sum of Ross Sea and Western Pacific Ocean (red line) and the reconstructed SIE (blue dashed line) are also shown. The solid black line and the solid blue line in the top panel represent the Southern Annular Mode (SAM) and Interdecadal Pacific Oscillation (IPO) indexes respectively. The corresponding dashed lines represent the 3-years running average. **(b)** Linear regression fit of the SIE (sum of September maxima of the Ross Sea and the Indian Ocean sectors) and log ($ssNa^+$ flux) for the time period ranging from 1979 to 2003. Pearson's *r* for the 23 data points used in the regression is 0.713. (For interpretation of the references to colour in this figure legend, the reader is referred to the web version of this article.)

flux (dark green line) and their 3-year running average (black dotted lines) over the 25-year long record. A general good agreement can be observed between the two series trends. The two main peaks at the beginning and end of the profiles seem to be in phase whereas is not always true for the smaller relative maxima in the middle of the records. Indeed, these 1-year shifts could be explained by a possible dating error due to the relatively low accumulation rate at Talos Dome site, which can be minimized by running averages but not completely excluded As already done by Iizuka et al. (2008), we compared the yearly averaged log ($ssNa^+$ flux) with the time series of September SIE maxima obtained from the sum of the Ross Sea and the Western Pacific Ocean both smoothed with a 3-year running average (see Fig. 5b). The value of the Pearson's correlation coefficient (*r*) was 0.713, statistically significant at 1%. Significance was calculated using two-tail *t*-test with a measure of effective degree of freedom as defined in Livezey and Chen (1983). The relationship between the SIE and the log ($ssNa^+$ flux) can be described by a simple linear regression according to this equation:

$$\text{SIE maxima}_{\text{Ross Sea + Southern Indian Ocean}}\ (10^6\ \text{km}^2) = 0.907 \times \log [ssNa^+\ \text{flux}]\ (\text{ng cm}^{-2}\ \text{a}^{-1}) + 4.12 \quad (1)$$

According to Eq. (1) we used our yearly-averaged $ssNa^+$ fluxes in order to calculate a modelled SIE maximum for each year in the time range between 1979 and 2003. The profile of this modelled Sea Ice Extent is shown as a blue dashed line in Fig. 5a. We observe a general agreement between the modelled and satellite-derived Sea Ice Extent, even if our simple linear model is not able to depict short-term variations (e.g. the 1990 or 1996 SIE peaks are completely missing).

Moreover, we can assess that for log ($ssNa^+$ flux) values similar to the present ones, we can reliably derive SIE maxima also in the past as already done at Talos Dome as a qualitative reconstruction by Buiron et al. (2012) for a time period spanning between 20.000 and 50.000 years BP (before 1950 AD). We have to keep in mind that the SIE calibration shown in this paper might not continue in a linear way beyond the range shown here.

The top panel of Fig. 5a shows the trends of the IPO and SAM indexes in the studied period, highlighting a general agreement among these two indexes and our reconstructed SIE. Using the 3-year averaged data for the IPO and SAM indexes (dashed lines in the top panel of Fig. 5a) and calculating the Pearson's correlation coefficient we found that $r = -0.44$ ($p < 0.0001$) and 0.61 ($p < 0.0001$) respectively.

Meehl et al. (2016) showed how Antarctic sea ice expansion since 2000s has been driven by Pacific decadal climate variability. Moreover several studies put in evidence the direct effect of IPO over West Antarctica and Antarctic Peninsula temperatures and in atmospheric circulation across the southern Pacific and Atlantic oceans. Conversely the IPO and $ssNa^+$ flux at TD site have similar trends over inter-annual period but the relative low correlation seems to suggest no other direct relationship.

On the other hand the teleconnection between SAM and $ssNa^+$ flux seems to be more pronounced. The Annular mode has been shifted towards more positive state since 1950s with a deepening of the Amundsen Sea Low near Antarctica which caused a more cyclone in the circumpolar through (Sinclair et al., 1997). This is consistent with the large spatial anti-correlation between GP and Na^+ flux shown in Fig. 3c. The coupling of favorable atmosphere dynamics and increase of surface where wind stress is able to blow up and transport toward coast sea salt could be the possible link between sea ice and Na^+ flux at TD site.

Fig. 6 shows the reconstruction of the September maximum SIE of the Ross Sea and Western Pacific Ocean sectors achieved by using our TALDICE dataset and the modelled SIE from the Ferrigno ice core (74°34′S, 86°54′W; Thomas and Abram, 2016) using MSA as a marker. The SIE reconstruction by Curran et al. (2003) from the Law Dome ice core (66°46′S, 112°48′E) and the Whitehall Glacier (72°54′S, 169°5′E; Sinclair et al., 2014) deuterium excess based SIE reconstructions are shown in Fig. 6 as well.

In order to compare our SIE reconstruction with the previously published works, we have to keep in mind that the three available ice core records used to reconstruct the past sea ice conditions, are influenced by different sectors of the Southern Ocean. The Law Dome reconstruction refers to the 80°E–140°E sector, covering the Western Pacific Ocean and a small part of the Indian sector, whereas at Ferrigno site MSA was found to depict the SIE across the Amundsen Ross sea, centred on 146° W. The WHG record, based on d-excess and MSA, depicts the Ross sea-ice conditions, overlapping the major part of our reconstructed area and for this reason represents the most interesting site to compare with TD.

The smoothed profile of the SIE at TD in Fig. 6 (solid black line) shows rather stable winter sea ice maxima over the

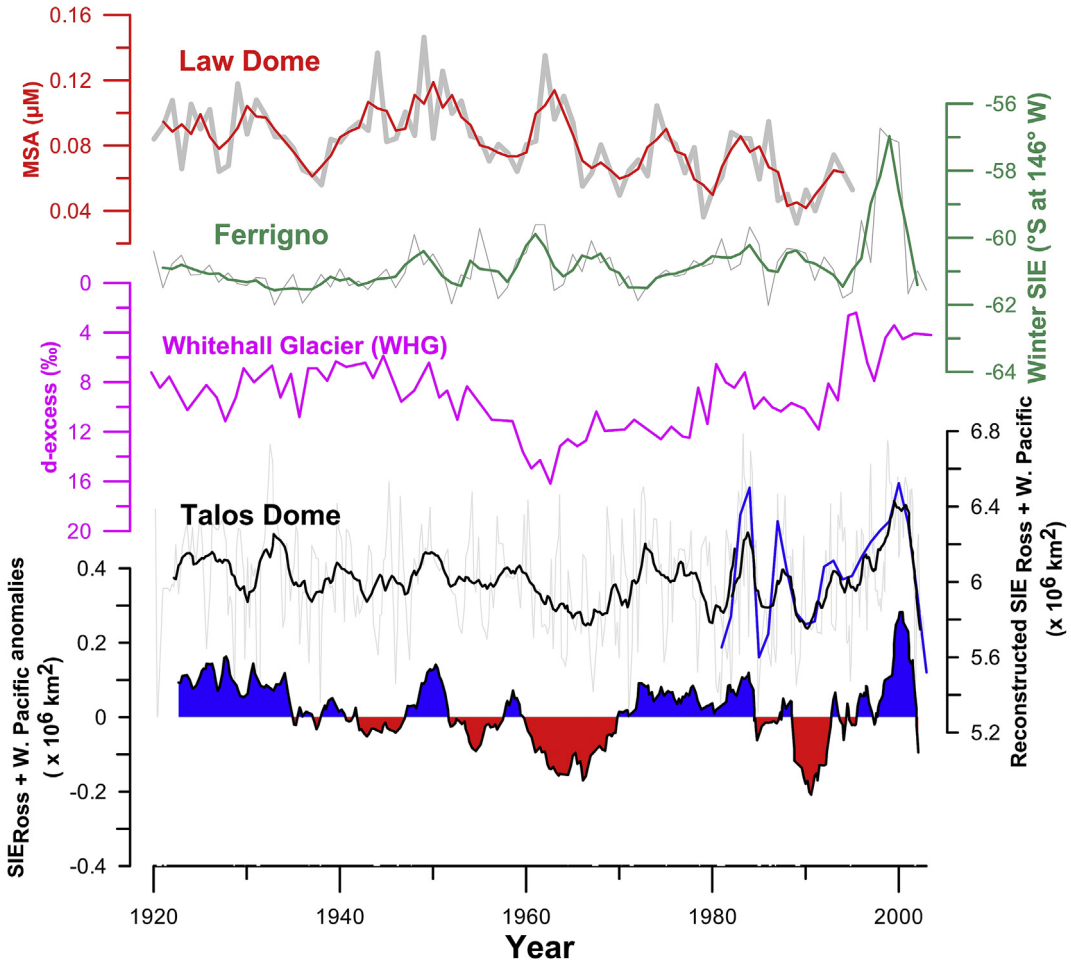

Fig. 6. Reconstructed SIE as the sum of the Ross Sea and Pacific sectors of the Southern Ocean between 1920 and 2003. The black solid line shows the 13-points smoothed profile obtained using our Eq. (1) and the $ssNa^+$ flux measured in the TALDICE ice core and in the snow pit sampled at Talos Dome (close to the TALDICE drilling site). The blue solid line shows the September SIE maxima as the sum of the Ross Sea and Pacific sectors of the Southern Ocean obtained by satellite measurements. The solid red line shows the 3-years running average of Law Dome MSA concentration as reported in Curran et al. (2003). The solid green line shows the 3-years running average of the SIE at 146°W as reconstructed by Thomas and Abram (2016). The solid magenta line shows the 3-year running average of the d-excess at WHG (rearranged from Sinclair et al., 2014). The bottom panel shows the SIE anomalies with respect to the 1920–2003 period. (For interpretation of the references to colour in this figure legend, the reader is referred to the web version of this article.)

1920–1960 period. Since the 1960s the SIE anomalies of our reconstruction with respect to the whole period (Fig. 6 - bottom panel) suggest an increased decadal-scale variability in the recent decades with respect to the beginning of the century as already found by Thomas and Abram (2016) in the Amundsen-Ross sea sector Furthermore, the reconstructed profile of the SIE in the Ross Sea and Western Pacific Ocean sectors highlights that SIE during the late 1990s was the greatest of the whole century, as observed in reconstructions by Thomas and Abram (2016) and Sinclair et al. (2014); during the late 1990s we can in fact observe the highest positive SIE anomalies over the last century (see bottom panel of Fig. 6).

The Law Dome record shows a continuous decline in the SIE starting from the 1950s and lasting to the end of the record; the onset of this decreasing trend in SIE is also visible in the Ross Sea sector as recorded in the TD and WHG reconstruction whereas it is not observed in the Ferrigno record. Despite the almost coeval beginning of this decreasing trend for TD, Law Dome and WHG reconstructions, we can observe an inversion in the SIE decline in the TD and WHG records starting from the late 1990s, when we have previously noticed the beginning of a negative phase of the IPO, whereas this inversion of trend is not visible in the Law Dome record.

4. Conclusions

We showed in this work that $ssNa^+$ flux in the Talos Dome region during a 25-year period spanning from 1979 to 2003 is consistent with the idea of using it as a proxy for reconstructing the Sea Ice Extension in the Ross Sea and Western Pacific Ocean, at least for recent decades. We found a statistically significant positive linear relationship between the log ($ssNa^+$ flux) and the SIE calculated by satellite data and through this relationship we were able to reconstruct the SIE profile directly from our $ssNa^+$ data for a 25-year long period. Therefore, we used this positive relationship, along with an assumption that the relationship is stationary, to reconstruct past SIE fluctuation for the 20th century, pointing out a higher variability of SIE from the 1960s. Moreover, we found that the last two decades show the highest SIE during the last century as already observed by other records. Using our approach, $ssNa^+$ could prove to be a proxy for SIE in this area, allowing to achieve a very high temporal resolution history of its past fluctuations for the last thousands years. Although our findings strongly support a relationship between $ssNa^+$ and SIE, it is also clear that meteorological conditions responsible for uplift and transport of sea-salt aerosol from the sea ice surface to the ice sheet have a strong influence on the $ssNa^+$ flux. Current and future efforts in sea salt aerosol

modeling will improve the understanding of the information hidden in the ssNa$^+$ ice core records.

Acknowledgements

This research was financially supported by the MIUR-PNRA program through a co-operation agreement among the PNRA consortium, University of Milano-Bicocca and University of Venice in the framework of the "Glaciology" and "Chemistry of Polar Environments" projects. This work is also a contribution to the ESF HOLOCLIP project. The HOLOCLIP Project, a joint research project of the European Science Foundation PolarCLIMATE programme, is funded by national contributions from Italy, France, Germany, Spain, Netherlands, Belgium and the United Kingdom. We thank the logistic and drilling TALDICE team. The Talos Dome Ice Core Project (TALDICE), a joint European programme led by Italy, is funded by national contributions from Italy, France, Germany, Switzerland and the United Kingdom. This is HOLOCLIP publication n° 29 and TALDICE publication n° 46.

References

Abram, N.J., Thomas, E.R., McConnell, J.R., Mulvaney, R., Bracegirdle, T.J., Sime, L.C., Aristarain, A.J., 2010. Ice core evidence for a 20th century decline of sea ice in the Bellingshausen Sea, Antarctica. J. Geophys. Res. -Atmos. 115, D23101. http://dx.doi.org/10.1029/2010JD014644.

Abram, N.J., Mulvaney, R., Arrowsmith, C., 2011. Environmental signals in a highly resolved ice ore from James Ross Island, Antarctica. J. Geophys. Res. 116, D20116. http://dx.doi.org/10.1029/2011jd016147.

Abram, N.J., Wolff, E.W., Curran, M.A.J., 2013. A review of sea ice proxy information from polar ice cores. Quat. Sci. Rev. 79 http://dx.doi.org/10.1016/j.quascirev.2013.01.011.

Allen, C.S., Pike, J., Pudsey, C.J., 2011. Last glacial-interglacial sea-ice cover in the SW Atlantic and its potential role in global deglaciation. Quat. Sci. Rev. 30, 2446–2458.

Armand, L.K., Crosta, X., Romero, O., Pichon, J.J., 2005. The biogeography of major diatom taxa in Southern Ocean sediments: 1. Sea ice related species. Palaeogeogr. Palaeoclimatol. Palaeoecol. 223 (1–2), 93–126.

Armand, L.K., Crosta, X., Queguiner, B., Mosseri, J., Garcia, N., 2008. Diatoms preserved in surface sediments of the northeastern Kerguelen Plateau. Deep- Sea Res. Part II 55 (5–7), 677–692.

Baldwin, M.P., 2001. Annular modes in global daily surface pressure. Geophys. Res. Lett. 28, 4115–4118.

Bazin, L., Landais, A., Lemieux-Dudon, B., Toyé Mahamadou Kele, H., Veres, D., Parrenin, F., Martinerie, P., Ritz, C., Capron, E., Lipenkov, V., Loutre, M.-F., Raynaud, D., Vinther, B., Svensson, A., Rasmussen, S.O., Severi, M., Blunier, T., Leuenberger, M., Fischer, H., Masson-Delmotte, V., Chappellaz, J., Wolff, E., 2013. An optimized multi-proxy, multi-site Antarctic ice and gas orbital chronology (AICC2012): 120–800 ka. Clim. Past. 9, 1715–1731. http://dx.doi.org/10.5194/cp-9-1715-2013.

Becagli, S., Proposito, M., Benassai, S., Flora, O., Genoni, L., Gragnani, R., Largiuni, O., Pili, S., Severi, M., Stenni, B., Traversi, R., Udisti, R., Frezzotti, M., 2004. Chemical and isotopic snow variability in East Antarctica along the 2001/02 ITASE traverse. Ann. Glaciol. 39, 473–482.

Becagli, S., Castellano, E., Cerri, O., Curran, M., Frezzotti, M., Marino, F., Morganti, A., Proposito, M., Severi, M., Traversi, R., Udisti, R., 2009. Methanesulphonic acid (MSA) stratigraphy from a Talos Dome ice core as a tool in depicting sea ice changes and southern atmospheric circulation over the previous 140 years. Atmos. Environ. 43 (5), 1051–1058. http://dx.doi.org/10.1016/j.atmosenv.2008.11.015.

Becagli, S., Lazzara, L., Marchese, C., Dayan, U., Ascanius, S.E., Cacciani, M., Caiazzo, L., Di Biagio, C., Di Iorio, T., di Sarra, A., Eriksen, P., Fani, F., Giardi, F., Meloni, D., Muscari, G., Pace, G., Severi, M., Traversi, R., Udisti, R., 2016. Relationships linking primary production, sea ice melting, and biogenic aerosol in the Arctic. Atmos. Env. 136, 1–15. http://dx.doi.org/10.1016/j.atmosenv.2016.04.002.

Belt, S.T., Masse, G., Rowland, S.J., Poulin, M., Michel, C., LeBlanc, B., 2007. A novel chemical fossil of palaeo sea ice: IP25. Org. Geochem. 38, 16–27.

Belt, S.T., Müller, J., 2013. The Arctic sea ice biomarker IP25: a review of current understanding and recommendations for future directions. Quat. Sci. Rev. 79, 9–25.

Bopp, L., Kohfeld, K.E., Le Quéré, C., 2003. Dust impact on marine biota and atmospheric CO2 during glacial periods. Paleoceanography 18 (2).

Bowen, H.J.M., 1979. Environmental Chemistry of the Elements. Academic Press, London.

Brandt, R.E., Warren, S.G., Worby, A.P., Grenfell, T.C., 2005. Surface albedo of the Antarctic sea ice zone. J. Clim. 18 (17), 3606–3622.

Buiron, D., Stenni, B., Chappellaz, J., Landais, A., Baumgartner, M., Bonazza, M., Capron, E., Frezzotti, M., Kageyama, M., Lemieux-Dudon, B., Masson-Delmotte, V., Parrenin, F., Schilt, A., Selmo, E., Severi, M., Swingedouw, D., Udisti, R., 2012. Regional imprints of millennial variability during the MIS 3 period around Antarctica. Quat. Sci. Rev. 48, 99–112.

Caiazzo, L., Becagli, S., Frosini, D., Giardi, F., Severi, M., Traversi, R., Udisti, R., 2016. Spatial and temporal variability of snow chemical composition and accumulation rate at Talos Dome site (East Antarctica). Sci. Tot. Env. 550, 418–430.

Cavalieri, D.J., Parkinson, C.L., 2008. Antarctic sea ice variability and trends, 1979-2006. J. Geophys. Res. - Oceans 113 (C7), C07004. http://dx.doi.org/10.1029/2007jc004564.

Collins, L.G., Allen, C.S., Pike, J., Hodgson, D.A., Weckström, K., Massé, G., 2013. Evaluating highly branched isoprenoid (HBI) biomarkers as a novel Antarctic sea-ice proxy in deep ocean glacial age sediments. Quat. Sci. Rev. 79, 87–98.

Criscitiello, A.S., Das, S.B., Evans, M.J., Frey, K.E., Conway, H., Joughin, I., Medley, B., Steig, E.J., 2013. Ice-sheet record of recent sea-ice behaviour and polynya variability in the Amundsen Sea, West Antarctica. J. Geophys. Res. 118, 1–13. http://dx.doi.org/10.1029/2012JC008077.

Curran, M.A.J., Van Ommen, T.D., Morgan, V., 1998. Seasonal characteristics of the major ions in the high-accumulation Dome Summit South ice core, Law Dome, Antarctica. Ann. Glaciol. 27, 385–390.

Curran, M.A.J., van Ommen, T.D., Morgan, V.I., Phillips, K.L., Palmer, A.S., 2003. Ice core evidence for antarctic sea ice decline since the 1950s. Science 302, 1203–1206.

Dieckmann, G.S., Hellmer, H.H., 2010. The importance of sea ice: an overview. In: Thomas, D.N., Dieckmann, G.S. (Eds.), Sea Ice, second ed. Wiley-Blackwell, Oxford, pp. 1–22.

Draxler, R.R., Rolph, G.D., 2012. HYSPLIT (HYbrid Single-particle Lagrangian Integrated Trajectory). NOAA Air Resources Laboratory, Silver Spring, MD. Model access via NOAA ARL READY. Website. http://ready.arl.noaa.gov/HYSPLIT.php.

Esper, O., Gersonde, R., 2014. New tools for the reconstruction of Pleistocene Antarctic sea ice. Palaeogeogr. Palaeoclimatol. Palaeoecol. 399, 260–283. http://dx.doi.org/10.1016/j.palaeo.2014.01.019.

Frezzotti, M., Urbini, S., Proposito, M., Scarchilli, C., Gandolfi, S., 2007. Spatial and temporal variability of surface mass balance near Talos Dome, East Antarctica. J. Geophys. Res. 112, F02032. http://dx.doi.org/10.1029/2006JF000638.

Foster, A.F.M., Curran, M.A.J., Smith, B.T., van Ommen, T.D., Morgan, V.I., 2006. Covariation of sea ice and methanesulphonic acid in Wilhelm II Land, East Antarctica. Ann. Glaciol. 44, 429–432.

Gersonde, R., Crosta, X., Abelmann, A., Armand, L., 2005. Sea-surface temperature and sea ice distribution of the Southern Ocean at the EPILOG Last Glacial Maximum – a circum-Antarctic view based on siliceous microfossil records. Quat. Sci. Rev. 24 (7–9), 869–896.

Iizuka, Y., Hondoh, T., Fujii, Y., 2008. Antarctic sea ice extent during the Holocene reconstructed from inland ice core evidence. J. Geophys. Res. -Atmos. 113 (D15), D15114. http://dx.doi.org/10.1029/2007jd009326.

Jones, J.M., Gille, S.T., Goosse, H., Abram, N.J., Canziani, P.O., Charman, D.J., Clem, K.R., Crosta, X., de Lavergne, C., Eisenman, I., England, M.H., Fogt, R.L., Frankcombe, L.M., Marshall, G.J., Masson-Delmotte, V., Morrison, A.K., Orsi, A.J., Raphael, M.N., Renwick, J.A., Schneider, D.P., Simp-kins, G.R., Steig, E.J., Stenni, B., Swingedouw, D., Vance, T.R., 2016. Assessing recent trends in high-latitude Southern Hemisphere surface climate. Nat. Clim. Chang. 6, 917–926.

Levine, J.G., Yang, X., Jones, A.E., Wolff, E.W., 2014. Sea salt as an ice core proxy for past sea ice extent: a process-based model study. J. Geophys. Res. Atmos. 119 http://dx.doi.org/10.1002/2013JD020925.

Livezey, R.E., Chen, W., 1983. Statistical field significance and its determination by Monte Carlo techniques. Mon. Wea. Rev. 111, 46–59. http://dx.doi.org/10.1175/1520-0493(1983)111.

Marshall, G.J., 2003. Trends in the southern annular mode from observations and reanalyses. J. Clim. 16, 4134–4143.

Massé, G., Belt, S.T., Crosta, X., Schmidt, S., Snape, I., Thomas, D.N., Rowland, S.J., 2011. Highly branched isoprenoids as proxies for variable sea ice conditions in the Southern Ocean. Antarct. Sci. 23 (05), 487–498.

Meehl, G.A., Hu, A., Santer, B.D., Xie, S.-P., 2016. Contribution of the Interdecadal Pacific Oscillation to twentieth-century global surface temperature trends. Nat. Clim. Change 6 (11), 1005–1008. http://dx.doi.org/10.1038/nclimate3107.

Morganti, A., Becagli, S., Castellano, E., Severi, M., Traversi, R., Udisti, R., 2007. An improved flow analysis—ion chromatography method for determination of cationic and anionic species at trace levels in Antarctic ice cores. Anal. Chim. Acta 603, 190–198.

Parkinson, C.L., Cavalieri, D.J., 2012. Antarctic sea ice variability and trends, 1979-2010. Cryosphere 6, 871–880. http://dx.doi.org/10.5194/tc-6-871-2012.

Rankin, A.M., Auld, V., Wolff, E.W., 2000. Frost flowers as a source of fractionated sea salt aerosol in the polar regions. Geophys. Res. Lett. 27, 3469–3472.

Roscoe, H.K., Brooks, B., Jackson, A.V., Smith, M.H., Walker, S.J., Obbard, R.W., Wolff, E.W., 2011. Frost flowers in the laboratory: growth, characteristics, aerosol, and the underlying sea ice. J. Geophys. Res.-Atmos. 116, D12301. http://dx.doi.org/10.1029/2010jd015144.

Röthlisberger, R., Mulvaney, R., Wolff, E.W., Hutterli, M.A., Bigler, M., Sommer, S., Jouzel, J., 2002. Dust and sea salt variability in central East Antarctica (Dome C) over the last 45 kyrs and its implications for southern high-latitude climate. Geophys. Res. Lett. 29 (20) http://dx.doi.org/10.1029/2002GL015186.

Sala, M., Delmonte, B., Frezzotti, M., Proposito, M., Scarchilli, C., Maggi, V., Artioli, G., Dapiaggi, M., Marino, F., Ricci, P.C., De Giudici, G., 2008. Evidence of calcium carbonates in coastal (Talos Dome and Ross Sea area) East Antarctica snow and firn: environmental and climatic implications. Earth. Planet. Sci. Lett. 271,

43–52.
Salinger, M.J., Renwick, J.A., Mullan, A.B., 2001. Interdecadal pacific oscillation and south pacific climate. Int. J. Climatol. 21, 1705–1721. http://dx.doi.org/10.1002/joc.691.
Sarmiento, J.L., Gruber, N., 2006. Ocean Biogeochemical Dynamics. Princeton University Press, Princeton.
Scarchilli, C., Frezzotti, M., Ruti, P., 2011. Snow precipitation at four ice core sites in East Antarctica: provenance, seasonality and blocking factors. Clim. Dyn. 37, 2107–2125. http://dx.doi.org/10.1007/s00382-010-0946-4.
Schlosser, E., Oerter, H., Masson-Delmotte, V., Reijmer, C., 2008. Atmospheric influence on the deuterium excess signal in polar firn: implications for ice-core interpretation. J. Glaciol. 54 (184), 117–124. http://dx.doi.org/10.3189/002214308784408991.
Serreze, M.C., Barry, R.G., 2011. Processes and impacts of Arctic amplification: a research synthesis. Glob. Planet. Change 77 (1–2), 85–96. http://dx.doi.org/10.1016/j.gloplacha.2011.03.004.
Severi, M., Becagli, S., Castellano, E., Morganti, A., Traversi, R., Udisti, R., 2009. Thirty years of snow deposition at Talos Dome (Northern Victoria Land, East Antarctica): chemical profiles and climatic implications. Microchem. J. 92, 15–20.
Severi, M., Udisti, R., Becagli, S., Stenni, B., Traversi, R., 2012. Volcanic synchronisation of the EPICA-DC and TALDICE ice cores for the last 42 kyr BP. Clim. Past. 8, 509–517. http://dx.doi.org/10.5194/cp-8-509-2012.
Simmons, A., Uppala, S., Dee, D., Kobayashi, S., 2006. ERA-Interim: new ECMWF reanalysis products from 1989 onwards. ECMWF Newslett 110, 25–35.
Sinclair, M.R., Renwick, J.A., Kidson, J.W., 1997. Low-frequency variability of Southern Hemisphere sea level pressure and weather system activity. Mon. Weather Rev. 125, 2531–2543.
Sinclair, K.E., Bertler, N.A.N., Bowen, M.M., Arrigo, K.R., 2014. Twentieth century sea-ice trends in the Ross Sea from a high-resolution, coastal ice-core record. Geophys. Res. Lett. 41, 3510–3516. http://dx.doi.org/10.1002/2014GL059821.
Smith, B.T., van Ommen, T., Curran, M.A.J., 2004. Methanesulphonic acid movement in solid ice cores. Ann. Glaciol. 39, 540–544.
Spolaor, A., Vallelonga, P., Plane, J.M.C., Kehrwald, N., Gabrieli, J., Varin, C., Turetta, C., Cozzi, G., Kumar, R., Boutron, C., Barbante, C., 2013. Halogen species record Antarctic sea ice extent over glacial-interglacial periods. Atmos. Chem. Phys. 13, 6623–6635. http://dx.doi.org/10.5194/acp-13-6623-2013.
Spolaor, A., Vallelonga, P., Turetta, C., Maffezzoli, N., Cozzi, G., Gabrieli, J., Barbante, C., Goto-Azuma, K., Saiz-Lopez, A., Cuevas, C.A., Dahl-Jensen, D., 2016. Canadian Arctic sea ice reconstructed from bromine in the Greenland NEEM ice core. Sci. Rep. 6, 33925. http://dx.doi.org/10.1038/srep33925.
Stenni, B., Buiron, D., Frezzotti, M., Albani, S., Barbante, C., Bard, E., Barnola, J.M., Baroni, M., Baumgartner, M., Bonazza, M., Capron, E., Castellano, E., Chappellaz, J., Delmonte, B., Falourd, S., Genoni, L., Iacumin, P., Jouzel, J., Kipfstuhl, S., Landais, A., Lemieux-Dudon, B., Maggi, V., Masson-Delmotte, V., Mazzola, C., Minster, B., Montagnat, M., Mulvaney, R., Narcisi, B., Oerter, H., Parrenin, F., Petit, J.R., Ritz, C., Scarchilli, C., Schilt, A., Schüpbach, S., Schwander, J., Selmo, E., Severi, M., Stocker, T.F., Udisti, R., 2011. Expression of the bipolar seesaw in Antarctic climate records during the last deglaciation. Nat. Geosci. 4, 46–49.
Thomas, E.R., Abram, N.J., 2016. Ice core reconstruction of sea ice change in the Amundsen-Ross Seas since 1702 A.D. Geophys. Res. Lett. 43, 5309–5317. http://dx.doi.org/10.1002/2016GL068130.
Thompson, D.W.J., Wallace, J.M., 2000. Annular modes in the extratropical circulation, part 1, Month-to-month variability. J. Clim. 13, 1000–1016.
Traversi, R., Becagli, S., Castellano, E., Larguini, O., Migliori, A., Severi, M., Frezzotti, M., Udisti, R., 2004. Spatial and temporal distribution of environmental markers from coastal to plateau areas in Antarctica by firn core chemical analysis. Int. J. Environ. Anal. Chem. 84 (6–7), 457–470.
Vallelonga, P., Maffezzoli, N., Moy, A.D., Curran, M.A.J., Vance, T.R., Edwards, R., Hughes, G., Barker, E., Spreen, G., Saiz-Lopez, A., Corella, J.P., Cuevas, C.A., Spolaor, A., 2016. Sea ice-related halogen enrichment at Law Dome, coastal East Antarctica. Clim. Past. Discuss. http://dx.doi.org/10.5194/cp-2016-74.
Veres, D., Bazin, L., Landais, A., Toyé Mahamadou Kele, H., Lemieux-Dudon, B., Parrenin, F., Martinerie, P., Blayo, E., Blunier, T., Capron, E., Chappellaz, J., Rasmussen, S.O., Severi, M., Svensson, A., Vinther, B., Wolff, E.W., 2013. The Antarctic ice core chronology (AICC2012): an optimized multi-parameter and multi-site dating approach for the last 120 thousand years. Clim. Past. 9, 1733–1748. http://dx.doi.org/10.5194/cp-9-1733-2013.
Wolff, E., Fischer, H., Fundel, F., Ruth, U., Twarloh, B., Littot, G.C., Mulvaney, R., Rothlisberger, R., de Angelis, M., Boutron, C.F., Hansson, M., Jonsell, U., Hutterli, M.A., Lambert, F., Kaufmann, P., Stauffer, B., Stocker, T.F., Steffensen, J.P., Bigler, M., Siggaard-Andersen, M.L., Udisti, R., Becagli, S., Castellano, E., Severi, M., Wagenbach, D., Barbante, C., Gabrielli, P., Gaspari, V., 2006. Southern Ocean sea-ice extent, productivity and iron flux over the past eight glacial cycles. Nature 440, 491–496.
Yang, X., Pyle, J.A., Cox, R.A., 2008. Sea salt aerosol production and bromine release: role of snow on sea ice. Geophys. Res. Lett. 35 (16), L16815. http://dx.doi.org/10.1029/2008gl034536.